Geophysical Journal (1989) **97**, 557–572

A high-resolution spectral study of audiomagnetotelluric data and noise interactions

A. Tzanis* and D. Beamish
British Geological Survey, Murchison House, West Mains Road, Edinburgh EH9 3LA

Accepted 1989 January 13. Received 1988 November 29; in original form 1988 January 12.

SUMMARY

This study is an investigation of the behaviour of audiomagnetotelluric (AMT) response estimates, in the presence of intense anthropogenic noise. The details of the data and noise interactions are studied by constructing highly resolved AMT response functions using the Maximum Entropy spectral analysis method, in its multichannel form. For low-noise, consistent data spectral estimates and their frequency resolution should be independent of the spectral technique used. Such behaviour is confirmed. When the data are contaminated by significant amounts of noise the highly-resolved estimates display detailed inconsistencies as a function of frequency. Such piecewise distortions can be understood if the response function is viewed as a polynomial. The results obtained enable the identification of response structure generated by both harmonic and subharmonic noise processes. High-resolution estimates provide a detailed view of data quality and narrow-band perturbations. The comparison of high-resolution response functions with conventional (discrete) estimates, shows that, in some cases, the latter may produce erroneous estimates. A discussion of the generation and received characteristics of noise waveforms is also included. A smoothing operation, involving frequency domain convolution, is described and applied to the results obtained. The technique exploits the minimum-delay properties exhibited by a valid impulse response function in the time domain.

Key words: electromagnetic induction, audiomagnetotellurics, noise, maximum entropy, spectral analysis.

1 INTRODUCTION

Conventional magnetotelluric data analysis requires the solution of the frequency domain equations:

$$E_x(f) = Z_{xx}(f)H_x(f) + Z_{xy}(f)H_y(f)$$
$$E_y(f) = Z_{yx}(f)H_x(f) + Z_{yy}(f)H_y(f) \quad (1)$$

or, in matrix form, $\mathbf{E} = \mathbf{ZH}$, where $\mathbf{Z}$ is termed the impedance tensor, or response function, and conveys information about the geoelectric structure in the vicinity of the recording station. The field components $\mathbf{E} = [E_x\ E_y]$ and $\mathbf{H} = [H_x\ H_y]$ are recorded in the time domain and form a mutually orthogonal set. The two pairs of impedance elements are usually estimated by least-squares solutions which minimize noise on a particular data channel (Sims, Bostick & Smith 1971). The quality of the least-squares solutions for each of the two pairs of impedance elements is then obtained from the multiple (predicted) coherence between the measured electric field component and that predicted by the least-squares solutions.

The auto- and cross-spectral estimates between the field components are conventionally computed using the Fast Fourier Transform (FFT) technique. Given the inherent variance of the resulting raw spectral density function, smoothing by averaging over a frequency interval, often arbitrarily chosen, is usually prescribed, in order to stabilize the spectral density estimates (band-averaging). The frequency resolution of the resulting impedance tensor estimates is thus drastically reduced. High frequency resolution will not, theoretically, offer additional information, because the impedance tensor (i.e. the Earth response) is a smooth function of frequency. However, few studies or examples of high-resolution impedance estimation have appeared in the literature. In addition, a highly resolved response will clearly display the effects of narrow-band spectral components that are extraneous to the induction process described by equations (1). This may ultimately assist in their identification and removal.

Noise problems are accentuated for data obtained in the audio and subaudio frequencies. The power distribution grid may contaminate the data with intense extraneous noise sources. The noise structure of a well balanced grid supply will be time-stable and comprise a fundamental (50 or 60 Hz) and associated line harmonics. Variable loads may also provide time-variable line sources and wide-band contamination. Powerful irregular transients also exist to provide additional narrow and wide band contamination. A

* Present address: 24 Agias Lavras St., Patisia, 111-41 Athens, Greece.

recent review of anthropogenic noise sources is provided by Menvielle & Szarka (1986).

In this study, we investigate some high-resolution properties of noise-contaminated EM data. We focus our attention on data from the lower audio frequencies, the so-called AudioMagnetoTelluric (AMT) data, as they are both more affected, and of more interest for upper crustal geoelectric studies. To obtain highly resolved and stable impedance estimates we have adopted the Maximum Entropy (MAXENT) spectral analysis method (Burg 1975; Jaynes 1982). High-resolution spectral estimation using the discrete Fourier transform appears in the robust spectral estimation techniques described by Chave, Thomson & Ander (1987). Such techniques may form a complementary non-parametric estimation procedure to the MAXENT method although they have yet to be applied to high-frequency/high-noise datasets.

In order to understand the behaviour of a high-resolution response function contaminated by noise, we first provide a description of the response function as a finite-degree polynomial. AMT data in the frequency range 0.1–100 Hz obtained at a number of sites in western Turkey are used to provide both conventional and high-resolution estimates of the impedance tensor. Although the two sets of results can be considered equivalent for certain (low-noise) data types, the high-resolution estimates display narrow-band structure for high-noise data. The results obtained are used to identify a number of 'inconsistent' features that arise due to the contaminating influence of noise. Noise sources, structured in frequency, appear to influence several portions of the spectrum. High-resolution spectral density functions of the data are also used to assist in our understanding of noise structure which appears to be generated by both harmonic and subharmonic processes.

The piecewise distortions of a response function are due to the convolution of the consistent data with inconsistent noise structure in several portions of the spectrum. All such discontinuities imply an unphysical response and identify inconsistent sections of the spectrum. The recovery of a consistent high-resolution response from such data requires careful consideration. For our data the noise structure is complex and it can only be understood *a posteriori*, using high-resolution procedures. Any attempt to remove piecewise distortion in the frequency domain involves a smoothing of the response function. The smoothing function must be consistent with known properties of the response function and it must not impose any other structure on it with no *a priori* information. A smoothing operation, involving convolution in the frequency domain, is suggested and applied to the results. The technique exploits the minimum-delay properties that must be exhibited by a valid impulse response function in the time domain.

2 THE RESPONSE AS A FINITE-DEGREE POLYNOMIAL

In the following discussion the concept of the polynomial response function in the time domain is used. This is an established result, although not always appreciated or explicitly stated. It follows from the fact that equation (1) must define a causal system. The linear dependence of an EM field component (e), on another orthogonal component (h), can only exist at preceding instances of time (lower case letters denote time domain processes). In general, this is described by the convolution

$$\begin{aligned} &e_t = h_t * z_t \\ &z_t = 0, \qquad t < 0 \end{aligned} \tag{2}$$

where z_t is the impulse response to EM excitation. The subscript t denotes discrete time. From equation (2) the alternative definition of z_t as mathematical filter can be deduced. The one-sided (causal/realizable) filter comprises a set of polynomial coefficients $z_t = (a_0, a_1, \ldots, a_j, \ldots)$ that contain information about the geoelectric structure. The one-dimensional (1D) conductivity distribution notation is implied for the sake of simplicity. The frequency transform of z_t is defined by the polynomial

$$\begin{aligned} Z(\omega) = \sum_{t=0}^{N} a_t \exp(i\omega t) = \sum_{t=0}^{N} a_t z^t \\ = a_N(z - z_1)(z - z_2)\cdots(z - z_N), \end{aligned} \tag{3}$$

where the z_j are the roots of $Z(\omega)$ and N is its order. In the frequency domain the fields are related as $E(\omega) = Z(\omega)H(\omega)$. The impedance filter is the inverse of the causal filter y_t which relates the field components as

$$\begin{aligned} &h_t = e_t * y_t \\ &y_t = 0, \qquad t < 0 \\ &z_t * y_t = \delta_t \end{aligned} \tag{4}$$

with y_t defined as the admittance filter. The two-way invertibility, implied by the last equation, necessitates that z_t be a minimum-delay wavelet, and equivalently that $Z(\omega)$ be a minimum-phase function (e.g. Robinson 1967; Clàerbout 1976). Thus the singularities of $Z(\omega)$ can only exist in the lower half ω-plane, and, all the zeros that exist on the imaginary ω-axis are necessarily simple. Finally, a definite property of all impedance and admittance functions is that, when they describe a passive system (no energy sources exist within the medium under consideration), they must have finite energy and positive dissipation over any time window from minus infinity up to any time t. Such properties require that the impedance/admittance impulse response be *positive real* (Claerbout 1976).

Given the inherent smoothness of a valid response $Z(\omega)$ and, assuming that there exists a finite (layered) conductivity profile, the *observable* geoelectric structure is a low order one and accordingly so is the associated polynomial impulse response. The very nature of the induction process smooths away small-scale perturbations. For discontinously recorded data, such as the band-limited decade system described later, the variation of $Z(\omega)$ per decade will seldom exceed an order of 3 or 4.

Having acknowledged the low degree of the finite response polynomial we are in a position to understand the effects of frequency variations introduced by noise, because the observed $Z(\omega)$ departs from its natural (low) degree as it is forced to adapt to the variable properties of the frequency domain. Thus additional poles and zeros are introduced. To investigate how this happens, let $N_E(\omega)$ and $N_H(\omega)$ be noise processes affecting the electric and magnetic field components respectively. Noise processes can

be classified as strictly or weakly stationary. The first kind refers to additive white noise. The second kind may incorporate all the natural and anthropogenic processes that are not due to passive EM induction, such as ground roll affecting the stability of the magnetic sensors. In all such cases the noise spectrum may be expressed in terms of a polynomial (e.g. Robinson 1980, p. 187), not necessarily minimum-phase or narrow-band.

Then the operation

$$Z(\omega) = \frac{E(\omega) + N_E(\omega)}{H(\omega) + N_H(\omega)}$$

defines a convolution in the time domain of z_t with n_{ht} so that

$$e_t + n_{et} = z_t * h_t + z_t * n_{ht}. \tag{5}$$

The result emerges as a polynomial of degree *at least equal* to that of $Z(\omega)$, i.e. the polynomial to which it has been added. If the noise sources define a polynomial of degree greater than that of $Z(\omega)$, (5) shows how additional zeros are introduced into the observed response. In the general case, the application of the parallel filter rule (e.g. Claerbout 1976; Robinson 1980) tells us what the relative effects of $N(\omega)$ are on $Z(\omega)$. The rule states that the frequency transform of the two processes has the same number of interior (to the unit circle) zeros (or equivalently the same number of zeros in the upper half ω-plane) as the transform of the dominant process. In particular, if the dominant process is minimum-delay, then the parallel combination of the processes will be minimum-delay; if it is mixed-delay, the combination will have a number of zeros in the upper half ω-plane and instability will occur. In other words, 'You can add garbage to a minimum-delay wavelet if you do not add too much' (Claerbout 1976). In normal circumstances, not too much is added, and a minimum-phase $Z(\omega)$ is recoverable. In the extreme case, however, $Z(\omega)$ will be contaminated by dominant mixed-phase processes introducing instability and structured variations, as well as white noise (i.e. a lot of garbage).

A conventional way of reducing the variance in standard frequency domain processing is to smooth the observed auto- and cross-spectral estimates of **E** and **H** by averaging over a usually arbitrary frequency interval. The spectral components of persistent noise souces will be included in the 'smoothed' spectrum and, if they are sufficiently powerful, will influence neighbouring frequencies. When dealing with such problems, our ability to identify the extent to which our data have been affected becomes important and brings forward the question of the frequency resolution of data processing. The problem of eliminating the noise structure is then left to a second-stage procedure. This study will be concerned with our understanding of a valid response and its recovery from data contaminated by a lot of garbage.

3 THE AMT DATA

In this study we are interested in the properties of data in the frequency range $0.1\,\text{Hz} < f < 100\,\text{Hz}$. The data were

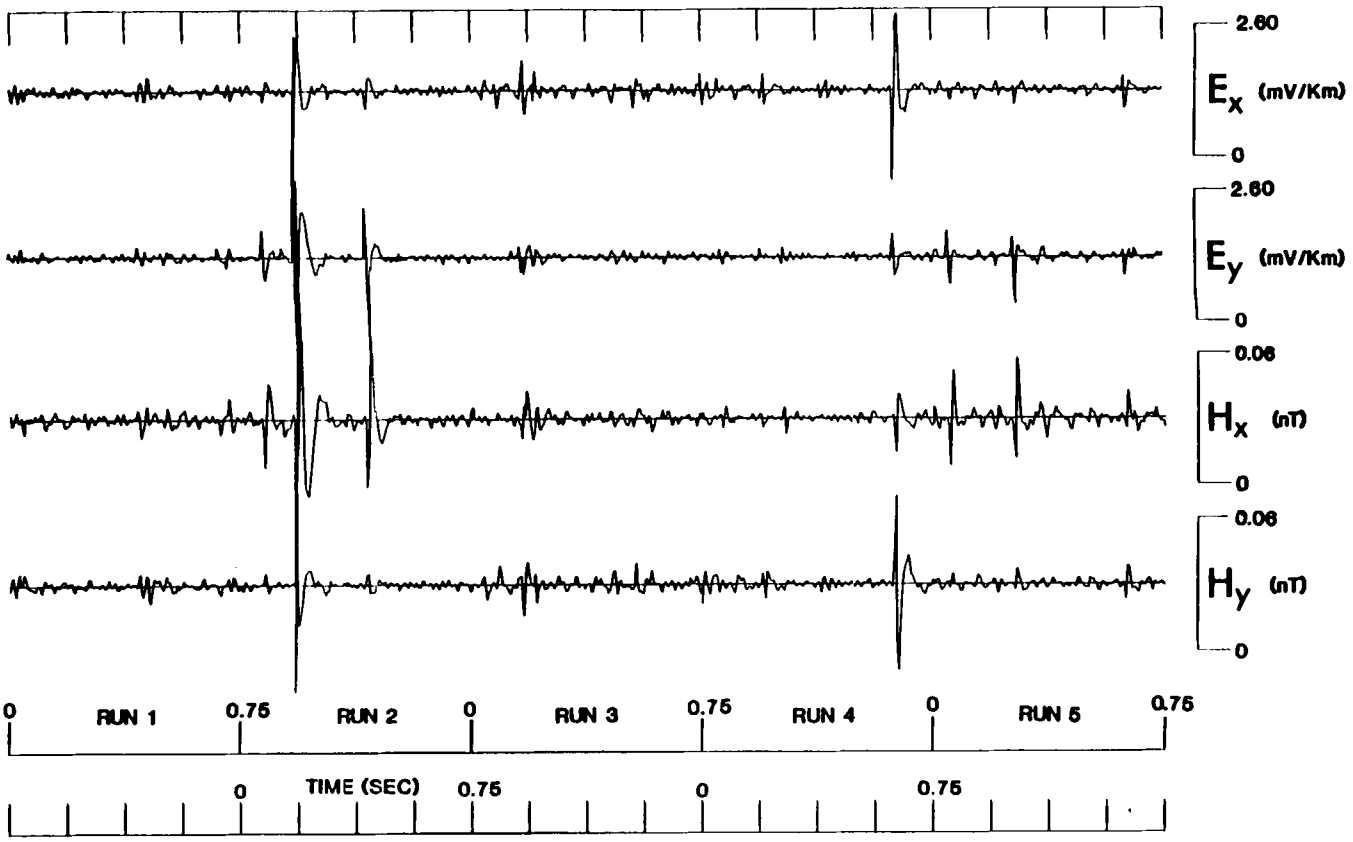

Figure 1. Four channels of decade 1 (100–10 Hz) data. Sampling rate is 200 Hz. Five successive data windows are shown each of 0.75 s duration. E_x and E_y are the N–S and E–W orthogonal components of the induced electric field respectively; H_x and H_y are the corresponding magnetic N–S and E–W components.

acquired with a computer-based AMT field system covering the bandwidth 0.01–100 Hz. Band-pass and notch filters were applied to condition the analogue signals prior to 12-bit digitization. The conditioning scheme provided four decades of data with sampling rates of 400, 40, 4 and 0.4 Hz across a window of 300 data points per decade. The data are resampled at 200, 20, 2 and 0.2 Hz across a window of 150 data points, so that the four decades cover the bandwidths 100–10, 10–1, 1–0.1 and 0.1–0.01 Hz, respectively. The time interval for the collection of each data window is thus 0.75, 7.5, 75, and 750 s, respectively. Collection took place in western Anatolia (Turkey), geographic coordinates 40.5 N, 30 E. Fig. 1 displays an example of decade 1 data (100–10 Hz) for five successive data windows (RUN numbers), in two orthogonal telluric and two orthogonal magnetic channels. The 100–10 Hz bandwidth is dominated by the Schumann resonance waveforms; in general they consist of transient events (sferics) representing the response of the Earth-ionosphere waveguide to extra-large lightning discharges, superimposed on a background due to the continuous global sum of lightning activity (e.g. Bliokh, Nikolaenko & Filippov 1980). It is evident that this data can be approximated by a sequence of locally stationary processes at best. Further details can be found in Beamish & Tzanis (1986) and Tzanis & Beamish (1987).

4 HIGH-RESOLUTION RESPONSE FUNCTIONS AND THEIR PROPERTIES

In the following we shall give examples of the properties of high-resolution response functions and compare the results with those based on the conventional FFT approach, for data recorded at different dates and at different locations. The high-resolution estimates were determined by the MAXENT method (Burg 1975; Jaynes 1982). The implementation of the multivariate MAXENT procedure and the assignment of error estimates through the least-squares solutions is described by Tzanis & Beamish (1987). The algorithm used is based on the work of Strand (1977). The most important feature of the multivariate procedure is that an Auto-Regressive (AR) model is determined *simultaneously* across all the data channels. The spectral parameters used in the analysis are (a) for MAXENT: data lengths of $N = 150$ fitted by AR models of order $M = 10$, unless otherwise stated, (b) for FFT: $N = 150$, cosine-tapered and extended to $N = 256$ by symmetrically appending zeros; variance reduction by averaging over 12 adjacent frequencies provides 9 response estimates per decade associated with 14 degrees of freedom. For the comparisons, data processing (other than spectral analysis) was *identical*. The impedance tensor elements were calculated by forming the weighted means of the individual element populations that passed a predicted coherence threshold of 0.80. Weights were the reciprocal variances associated with each element. Upward- and downward-biased elements were treated separately and subsequently combined to produce the 'unbiased' result displayed. We show the modulus of the unrotated off-diagonal impedances (logarithmic scale) and their associated phase response as a function of frequency (logarithmic scale). Errors refer to one standard deviation throughout.

Example site 1

Two decades of the off-diagonal impedance function from site 1 are presented in Fig. 2. The MAXENT estimates with their upper and lower bounds (±1 s.d.) are represented by the continuous curves. The corresponding FFT results are represented by discrete symbols. The main inconsistent features observed are indicated by numbers 1, 2 and 3. *Feature 1* covers the 8–10 Hz range. It is less evident in the modulus of the impedance function and more impressive in the sloping phase response; the unconformity between the two decades is apparent in the divergence of the phase. This is a combined effect caused by instrumental filters and, mainly, by (the principal) aliases of the power grid fundamental. The phenomenon requires special attention and will be discussed later in more detail. *Feature 2* is the effect of a strong residual noise component due to the power distribution grid that leaked through the sidelobe structure of the 49 Hz instrumental notch filter because of its unstable harmonic content. Thus, it can be seen to affect the bandwidth between 43 and 62 Hz, and is more extreme in the Z_{xy} component. Feature 2 is a case of noise differentially affecting the field components. *Feature 3* is a scaled down version of Feature 2, which we believe is due to the first harmonic of the unstable mains fundamental. It is centred at 97.9 Hz, affecting the 92–100 Hz bandwidth; it possesses similar time-dependent characteristics. The qualitative and quantitative difference on the two elements is obvious.

There is another interesting effect that can be resolved with such a data adaptive technique. Consider Fig. 2, in which the solutions obtained with MAXENT and FFT techniques are compared. In Fig. 2(a), the decade 1 impedance has been evaluated from data affected by the mains harmonics. In Fig. 2(b) the decade 1 impedance has been evaluated from 'cleaned' data with the mains harmonics and their sidelobe structure removed through time-domain inverse filtering; details of this procedure are described in Tzanis (1987). In Fig. 2(c), solutions obtained with MAXENT for *noisy* data are compared with those obtained with FFT for *clean* data. The decade 2 (10–1 Hz) solutions are the same for both techniques. It is apparent that the decade 2 solutions obtained with both techniques are in good agreement and display a structured spectrum in both amplitude and phase, indicating localized interference. Note the behaviour of the 1–3 Hz bandwidth in particular. As can be seen in Fig. 2(a) the decade 1 amplitude response functions evaluated by either spectral method agree apart from the 10–20 Hz bandwidth. This is not the case for the phase response. The FFT phase appears to be downward shifted with respect to the MAXENT phase. From Fig. 2(b) we observe that this effect no longer occurs for '*clean*' data, and the phase responses are in very good agreement. Furthermore, from Fig. 2(c), the *clean* FFT response and the *noisy* MAXENT response *match* fairly well. It would appear that the phase response obtained with FFT for the noisy data is an incorrect function, while the MAXENT phase is more consistent. The downward pointing arrows in the phase diagram of Fig. 2(a) indicate the average positions of the strong residual (53.4 Hz) mains component and what appears to be the effect of its associated sideband and/or subharmonic structure. They are seen as smooth undulations superimposed on the 'true' phase movement at the vicinity

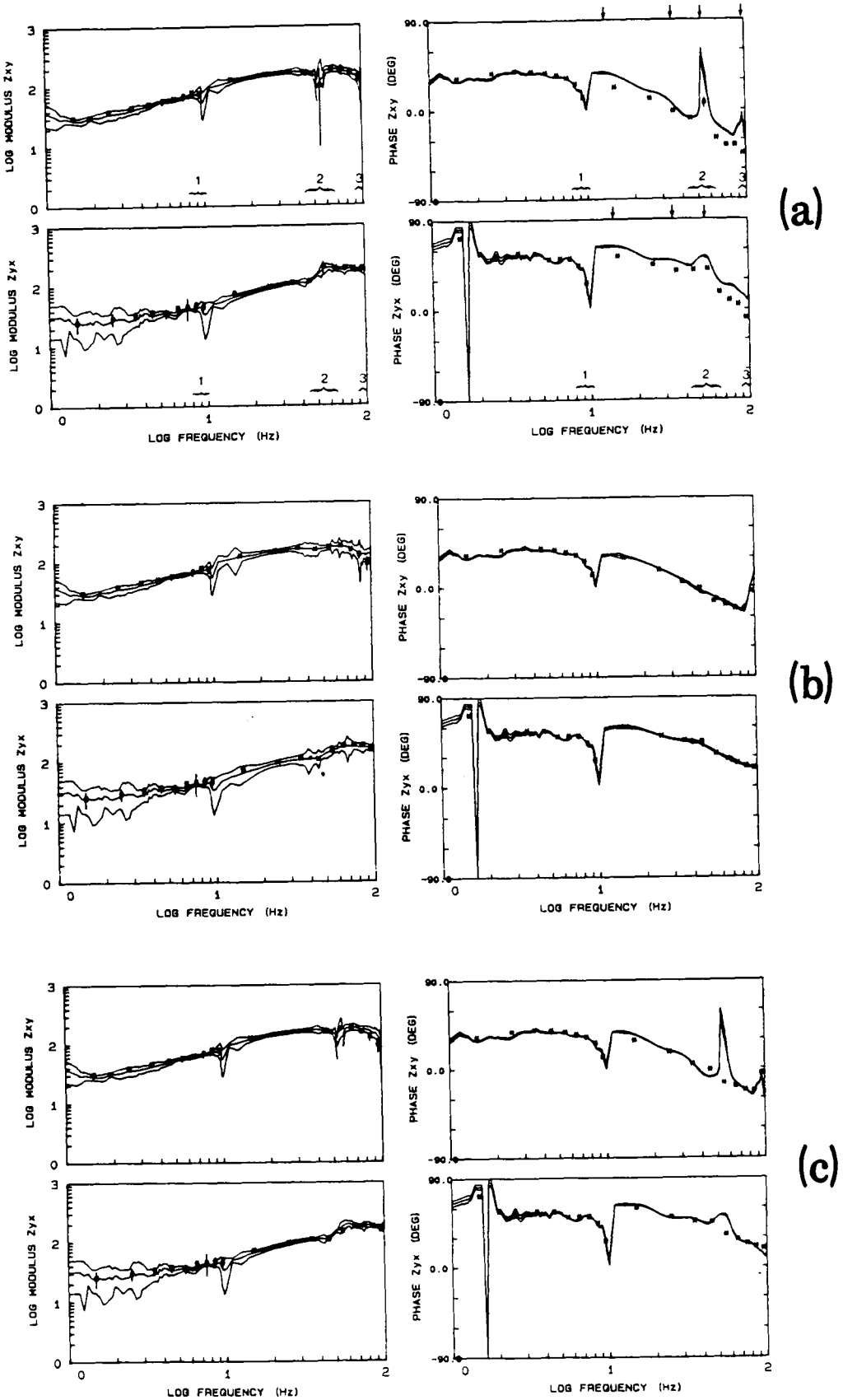

Figure 2. Demonstration of the performance of MAXENT spectral analysis in AMT impedance estimation—comparison with FFT-based analysis, for example site 1 data. MAXENT results are continuous lines (estimate ±1 s.d.), FFT results are discrete symbols with error bars (±1 s.d.); if no error bar is shown it is smaller than the symbol. Bandwidth shown extends from 1 to 100 Hz. Impedance values in units of $mV\,km^{-1}\,nT^{-1}$. Comparisons of impedances are: (a) From the original field data contaminated by noise due to power distribution grid. (b) From the same data but noise affecting decade 1 (100–10 Hz) removed. (c) From contaminated data (MAXENT) and 'clean' decade 1 data (FFT).

of 12, 30, 50 and 98 Hz. It must be appreciated that resolution down to the level of the noise spectral lines is not possible because of their low power level and the dispersive filtering effect of the Earth. What we are actually observing is their combined interference effect. It could be that spectral averaging over a bandwidth containing a rapidly moving phase, and structured noise components, introduces harmonic distortion and phase shifts. When we compare the response obtained by the two spectral methods for the cleaned dataset however (Fig. 2b), we see that they are almost consistent. For noise-free, consistent data, the determination of the response functions should be independent of the spectral analysis technique and this is what we observe.

Example site 2

The data obtained at site 2 are affected by a moderate mains harmonic (50 Hz) and its associated higher and lower order structure, with a stronger component in the E–W direction. The quality of the data was good with more than 70 per cent of the recorded data windows possessing predicted coherences >0.80. Two decades of the off-diagonal impedance function from site 2 are presented in Fig. 3. The amplitude response for this site is a smooth, well-behaved function of frequency, but again, the most interesting features appear in the highly structured (ripple-like) phase response, particularly in the first decade (Fig. 3a). Here as well, the crests of the ripples are believed to correspond to

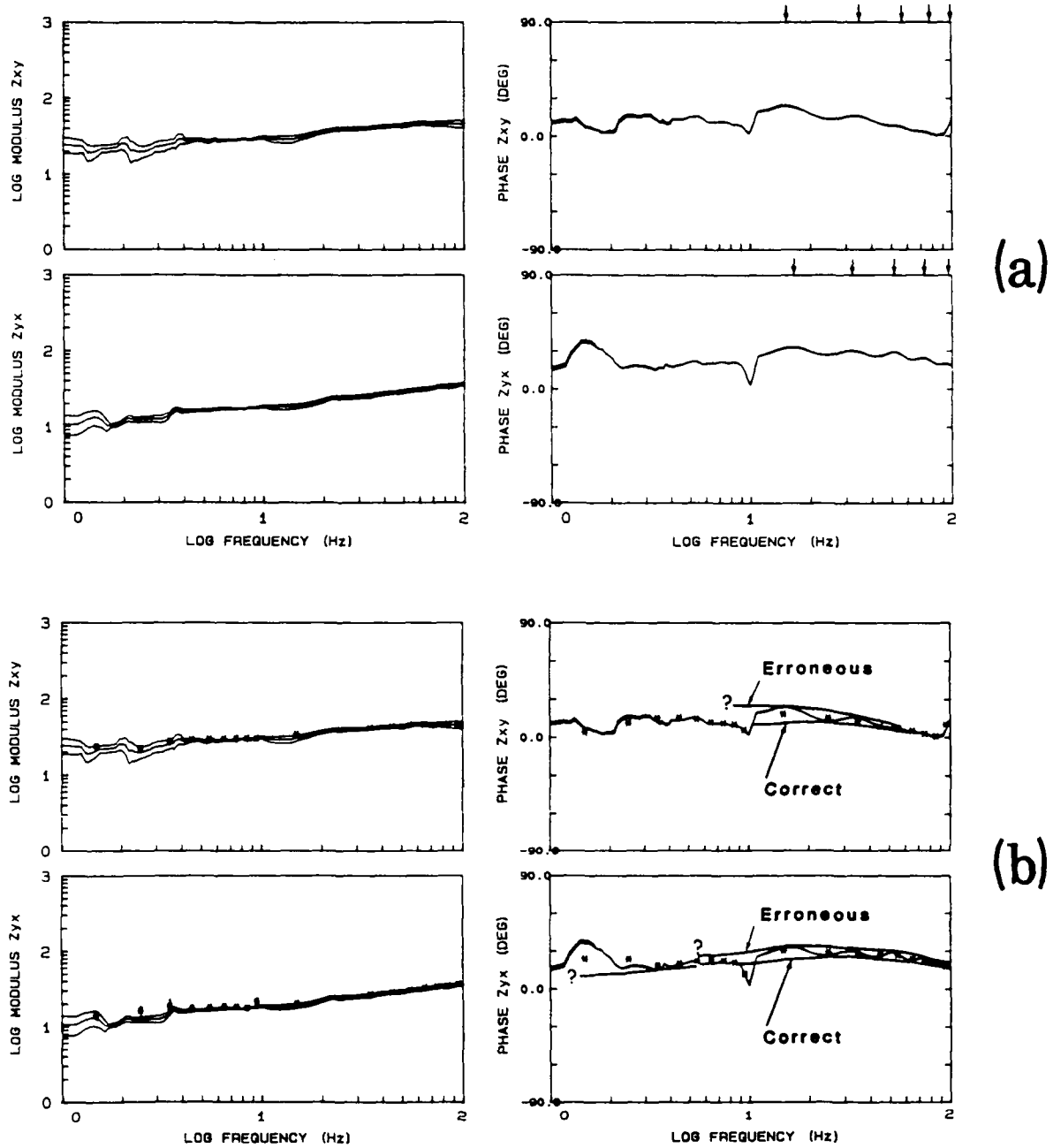

Figure 3. As Fig. 2 but for example site 2. The results shown are: (a) High-resolution impedance functions from data contaminated by weak mains noise sources. (b) Comparison between MAXENT and FFT response functions for same data.

the effects of the mains associated harmonic structure (near 10, 30, 50 and 100 Hz), subject to the same resolution constraints as site 1. An additional feature is present at about 70 Hz and is of unknown origin. The troughs again correspond to the relatively unaffected frequency components. However, the fundamental (50 Hz) harmonic appears very weak, in contrast to that at site 1. The noise effects are more intense in the Z_{yx} tensor element and are more pronounced because of the relatively flat 'true' phase response upon which they are superimposed. Decade 2 displays the same 8–10 Hz distortion as site 1. Structure is also observed in the decade 2 Z_{yx} tensor element with properties similar to those at site 1.

Figure (3b) displays the correspondence between FFT- and MAXENT-derived impedance functions. A good agreement between them is immediately apparent in both amplitude and phase. The flat and smooth nature of the latter does not give rise to shifting problems as at site 1. The FFT-phase estimates appear to be consistent averages of a continuous (MAXENT) response curve. This however means that they contain erroneous as well as valid contributions and, as a result, they are not correct estimates of the true phase. The frequency components near the troughs of the ripple structure apparently provide more reliable estimates of the true phase response. In fact two asymptotic bounds can be drawn for the MAXENT-phase data, as shown in Fig. 3(b). These correspond to the 'correct' and 'erroneous' response, and can be compared with the FFT results. The differences are not trivial; if we are in a position to obtain error bounds accurate to within 5 per cent, any modelling of the response obtained may produce misleading results if incorrect estimates are used.

Example sites 3 and 4

The third example is used to emphasize some difficulties that can arise when the conventional method of smoothing the auto- and cross-spectral estimates, by band-averaging, is applied in cases of severe frequency local noise contamination. The example is for decade 3 (0.1–1 Hz) data and was

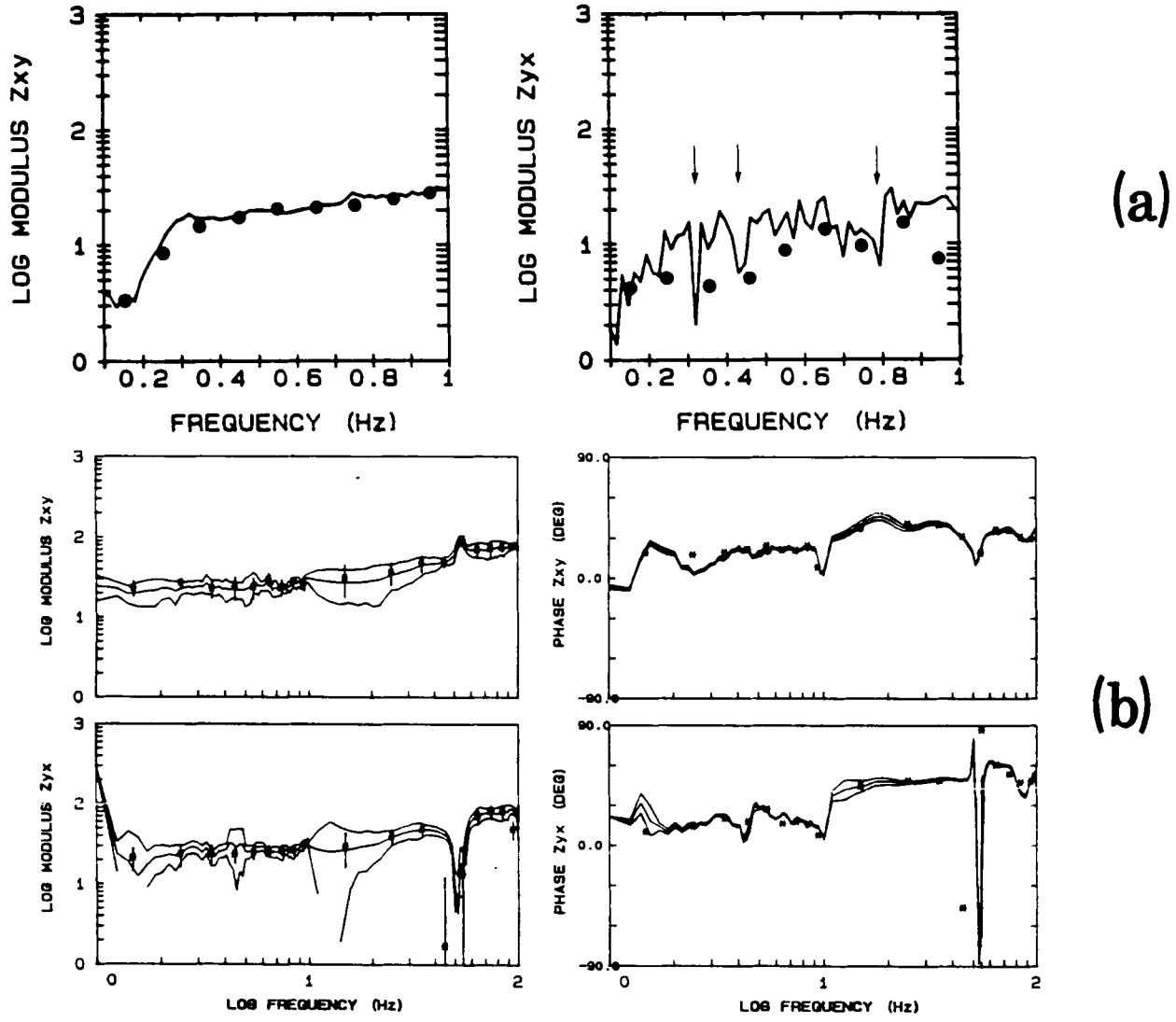

Figure 4. Comparison between MAXENT and FFT response functions at example sites 3 and 4. Impedance values in $mV\,km^{-1}\,nT^{-1}$. (a) The modulus of the high-resolution (continuous line) and the discrete (FFT) impedance function (solid circles), at example site 3. No error estimates are shown. (b) The modulus and phase of the high-resolution (continuous line) and the discrete (FFT) impedance function (stars) at example site 4.

recorded in a very high noise environment with directional (E–W) characteristics. The noise possessed two features; it comprised random, low amplitude spikes, and structured harmonic processes at the vicinity of 0.1, 0.32, 0.45 and 0.7–0.85 Hz. Such noise structure is very similar to that observed for the decade 3 data of site 1, the received spectra of which are displayed and discussed in Fig. 6. The modulus of the Z_{xy} and Z_{yx} elements of the impedance tensor are shown in Fig. 4(a). We present overlaid plots of the high resolution (MAXENT) and the FFT results. For the sake of clarity, error estimates and phase responses are not shown. The mutually consistent natue of the MAXENT and FFT results, for the adequately estimated Z_{xy} element, can be observed. However, this is not the case for the Z_{yx} element. The locations of the structured noise components are evident from the large amplitude spikes, indicated by arrows. In addition the averaged FFT spectra display considerable downward-bias due to the consistent nature of the spectral contamination; band averaging over closely spaced noise components allows the noise to dominate the data. The MAXENT spectrum does not, of course, avoid these complications. It can be seen that the low frequency response appears corrupted for both Z_{xy} and Z_{yx} components. We make this inference because we consider the steep gradient of the impedance to be unphysical, over such a narrow bandwidth. Except for this common feature, the rest of the Z_{xy} component is a smooth and stable function of frequency. In the Z_{yx} element, we observe that several portions of the bandwidth are left relatively unaffected by the structured noise components, and are therefore, marginally recoverable. High-resolution estimation allows a 'frequency-localized recovery' of the adequate data properties.

Note that the above discussion is not meant to suggest that the FFT spectral technique is an unwarranted procedure to apply when 'structured' noise spectra are present. In all normal circumstances, and for most 'noisy' cases, the two techniques return consistent results, and we are prepared to accept that there may be cases where the FFT spectral procedure may be more stable. In order to reassert this point, at least for the harmonic noise problem, in Fig. 4(b) we present overlaid plots of the impedance functions returned by both spectral techniques for a different site, example site 4. The site apparently suffers from more extreme noise conditions than the first two examples, but both techniques return mutually consistent results. This indicates that it is the local combination of noise and data statistics that determines whether problems such as those described above will actually occur. This is somewhat unfortunate because no prior information about such interactions is possible and defines the degree of caution that must be exercised while analysing and interpreting data recorded in intense noise regimes.

Noise correlations (example sites 5 and 1)

In the above presentation we have demonstrated the existence of structure in the impedance spectra and interpreted it as the result of structured noise interference. We have also acknowledged that part of this interference is due to the mains harmonic and subharmonic structure. In this section we investigate the causes of these effects by comparing the 'received' characteristics of our data.

One basic question is how can subharmonic interference be produced, or, equivalently, what is the frequency divider(s) producing it? The explanations we can offer are limited to the level of our undersanding of the processes involved in the complex pattern of noise generation and propagation. However, we are in a position to present evidence corroborating subharmonic generation due to an unstable power distribution grid. Figs 5(a) and (b) show decade 1 (100–10 Hz) and decade 2 (10–1 Hz) data obtained at a fifth location (example site 5). The two components of the telluric field are presented. The data were recorded quite near to a power distribution substation. For these data, the instrumental (50 Hz) notch was applied to the E_x component but not for the E_y component. The enormous 2.3 V km^{-1} sinusoid observed along the E–W direction (E_y) is therefore the actual signal emitted by the grid. The N–S (E_x) component displays the effects of the application of the instrumental (50 Hz) notch filter, intended to counter this particular noise problem. In addition, the noise along both directions appears to be amplitude modulated. Fig. 5(c) displays the MAXENT spectra of an accumulation of 165 data windows for both decades, in the E_x and E_y components. The spectrum of the fundamental mains harmonic can be seen to exist in two distinct modes, at 48.8 and 51 Hz (E_y component). These modes could possibly be interpreted as eigenfrequencies of an unstable mains grid, resulting from short-term variations of the fundamental. In turn, they can be used to explain most of the features observed in the decade 1 data, as they will provide a superposition of waves travelling with different relative frequencies. The asynchronous operation of motors can produce more sidebands and subharmonics of the mains emissions and may contribute towards this effect. The net result will be the emergence of a wavepacket displaying amplitude modulation as observed in the data, and the generation of the 98 Hz harmonic, as well as a series of subharmonics. The $n = 2$ (25 Hz) subharmonic is clearly observable in the E_x spectrum, while both the $n = 2$ and $n = 3$ (12.5 Hz) subharmonics are evident in the E_y component (note the scale size). It must also be appreciated that the power associated with this subharmonic structure will be variable with time, and associated with the propagation properties of the wavepacket. Therefore, their effect can be underestimated in such a time-averaged spectrum.

The emerging wavepacket appears to travel with a given group velocity on a carrier frequency with unstable characteristics. As a result, noisy power could leak into lower frequency bands, in the form of a wavepacket envelope. Such an effect can be observed in the 4–8 Hz frequency range of Fig. 5(c). Recall that the E_x telluric component was recorded with the instrumental notch operational for both decades. The reduction of the power level at about 50 Hz, causes considerable reduction of leakage into decade 2; hence the qualitative difference from the E_y component, recorded with the notch 'out'. An approximately 2 orders of magnitude difference in the power level is evident, while the shape of the spectrum approaches the theoretically expected one, displaying a minimum in this frequency range. The instability of the power distribution

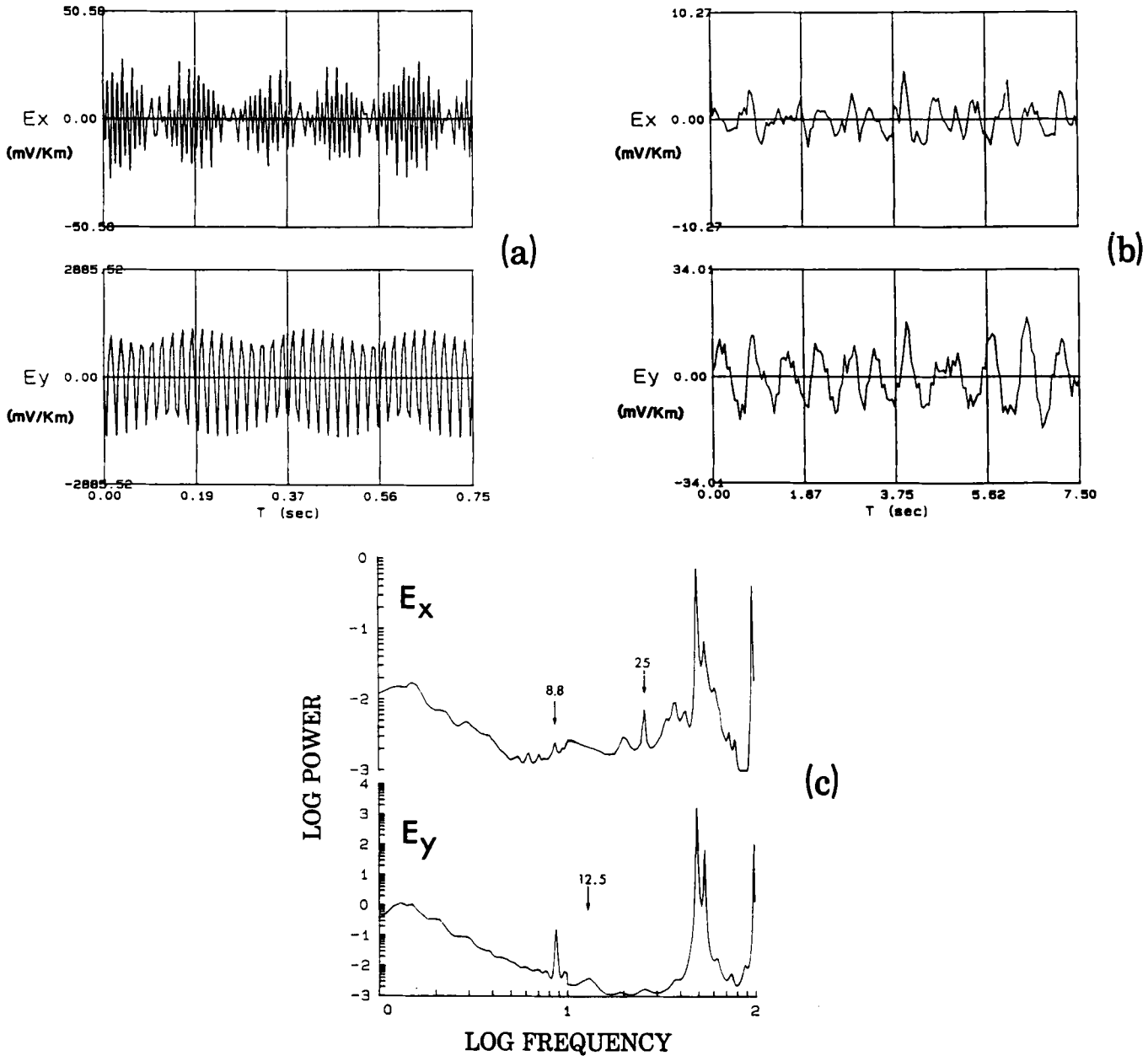

Figure 5. Examples of mains-noise contaminated data near a probable source at example site 5: (a) Decade 1 data (100–10 Hz). (b) Decade 2 data (10–1 Hz). (c) The time averages of the E-field power spectral density functions (units $(\text{mV km}^{-1}\,\text{nT})^{-2}\,\text{Hz}^{-1}$) at example site 5. Bandwidth is from 1 to 100 Hz. Single channel MAXENT spectral analysis of 165 successive data windows for each decade. Data lengths of $N = 150$ and AR operator lengths of $M = 30$ were used throughout.

grid appears to provide the frequency dividers required for subharmonic generation.

Consider now the spectral line observed in the decade 2 E_y telluric component, at 8.8 Hz (indicated by the arrow). This feature cannot belong to the fundamental Schumann resonance mode, because (a) it is too powerful, and (b) its Q factor is too high (>20). The Q factors of the Schumann resonances reflect the very low transmission coefficient of the ionosphere; they should in general be <8 (e.g. Bliokh *et al.* 1980). We believe that this spectral line may be interpreted as an alias of the 48.8 Hz mains mode. The folding of aliasing frequencies into lower frequency bands is given by the expression

$$f_a = f - 2mf_N, \qquad m = 1, 2, \ldots$$

with f_N representing the Nyquist frequency. For decade 2 data $f_N = 10$ Hz and therefore the generation of the aliased component at 8.8 Hz can be explained. Again it is interesting to observe the effect of the notch filter on the aliased power level of the E_x telluric channel. The power of the 48.8 Hz peak is reduced by almost 4 orders of magnitude. Accordingly, the aliased power level is drastically reduced. However, enough of it remains to fold back into decade 2 and form a low amplitude aliased

spectral component. This is important in that it offers the most probable explanation for 'Feature 1' observed in our earlier presentation of impedance functions.

It is interesting to note that the results presented above in the form of observed spectra can very easily be simulated with a simple superposition of sinusoids at nominal frequencies of 49 and 51 Hz in additive noise. We have been able to reproduce several of the effects cited above. Having established the possibility of wide-band data contamination by narrow-band unstable noise processes, we proceed to examine their 'received' characteristics for site 1. Fig. 6 shows the MAXENT spectra for the two telluric (E_x, E_y) and magnetic (H_x, H_y) components for this site. We present 3 decades of spectra for reasons that will become apparent later. Spectral levels at decade boundaries are necessarily discontinuous. In decade 1, we observe that the most prominent features are the spectral lines at 53 and 98 Hz, and the consderable reduction in power level *c* 50 Hz caused by the instrumental notch. The former lines are again an effect of an unstable power distribution grid, for which the instrumental filter was no match. Apart from these two large-scale features no other directly identifiable noise effect is observed in the spectrum. The most interesting features can be seen in the spectral structure of the 7–40 Hz frequency range. Here we observe a complement of the first 6 Schumann resonance modes (typically 7.8, 14.0, 21.0, 27.0, 33.5 and 39.5 Hz for modes $n = 1$–6). They are most clearly seen in the H_x magnetic component. The Q factors associated with all these peaks are of the right order of magnitude (<8); problems however are still abundant, especially in the telluric channels. For the $n = 1$ mode these materialize in the form of an aliased spectral component (indicated by up arrows), contaminating the 8–10 Hz bandwidth. For the higher order modes the situation is more complicated. It must be appreciated that at the level of attainable frequency resolution, subharmonic interference could easily be hidden in the resonant spectral peaks. For example, the 25 Hz subharmonic would easily be incorporated to the $n = 4$ spectral structure. Likewise, the $n = 2$ (14 Hz) resonance and the 12.5 Hz subharmonic occupy adjacent frequency locations and could readily merge. Thus, the power spectrum appears at first to be consistent. Closer inspection would reveal the existence of small differences in the location of spectral peaks, notably for the $n = 2$ (indicated by broken vertical line) and higher ($n = 5, 6$) modes. Therefore, although individual spectral lines due to noise are not observed, we believe that it is their influence that causes the spectral inconsistency and the ripple in the phase of the response functions for this frequency range.

The lower frequencies in Fig. 6 display a stable spectral structure throughout the whole 0.1–8 Hz frequency range. Here we observe some similarities in the location of some spectral features for the decade 2 and 3 spectra; the numbered arrows indicate peaks that appear to be located in frequency multiples of 10 with respect to each other. We cannot account for the existence of these frequency multipliers (or dividers). Spectral peaks that appear consistent over the four data channels are indicated by down arrows. An appreciable amount of power appears to exist in the 3–7 Hz range, particularly in the E_x and H_y channels. Most of the features observed are unaccounted for by theory. We are inclined to label them as man-made

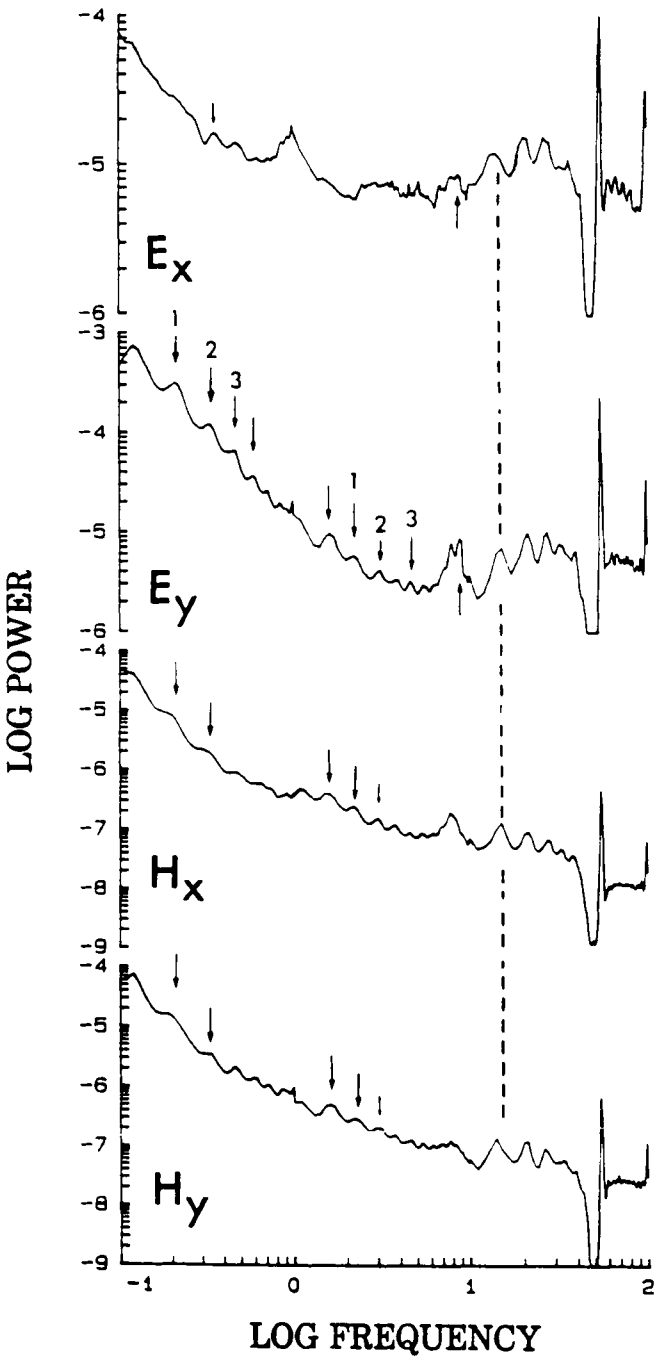

Figure 6. Three decades of the time-averaged power spectral density functions of the four horizontal components of the EM field, at example site 1. Bandwidth is from 0.1 to 100 Hz. Units for E fields are $(\text{mV km}^{-1}\text{ nT})^{-2}\text{ Hz}^{-1}$. Units for H fields are $(\text{nT})^2\text{ Hz}^{-1}$. Single channel MAXENT spectral analysis of 165 data windows (decades 1 and 2) and 100 data windows (decade 3). Data lengths of $N = 150$ and AR operator lengths of $M = 30$ were used throughout.

interference, and we believe that enough coherent contributions may pass the established acceptance tests and produce the kind of distortions we observe.

Discussion of results

From the results presented, it appears that data adaptive spectral estimation techniques such as MAXENT when

applied to EM data produce response functions with properties which are highly localized in frequency. The high resolution affordable by these techniques may be used to improve our insight into some of the processes involving the signal and noise interactions, enabling a better understanding of their behaviour. When the data are contaminated by narrow-band interference, the high resolution afforded by MAXENT appears to enable the extraction of undistorted portions of the bandwidth. Instrumentation cannot always cope with the challenges presented by noise and the requirements of smoothing may integrate very uncomforting spectral contributions.

In terms of the contaminated impedance polynomial the main problems encountered were due to structured processes, superimposed on that due to passive natural induction, for which a polynomial representation can always be constructed. The piecewise distortion of the response curve results from its multiple convolutions with such noise components. Feature 1 (8–10 Hz) provides an excellent example of such an interaction. It is well known that analogue bandpass filters (in this case 8-pole Butterworth), have a maximum-delay phase response. The aliased components, with power at least equivalent to that of the data, provide an additional destabilizing agent in the near-Nyquist band. The parallel filter rule then demands that the resulting 'noise' wavelet be of maximum-phase. The same rule requires that its convolution with the Earth response be at least of mixed-phase. The abrupt departure of the observed phase from its prescribed smooth minimum movement is a clear manifestation of this effect. A rapid amplitude and phase movement is observed in the data interaction with the mains harmonics and its associated spectral structure. We note here that a minimum-phase wavelet can be extracted by MAXENT for these components. The parallel filter rule again demands that the poles and zeros of the dominant filter dictate the behaviour of the system. Therefore, upon frequency transformation, the local integration contour is deformed so as to include the poles of the power distribution grid system. The resulting impedance movement may be minimum for the combined system, albeit spurious and unphysical.

Similar arguments can be used to explain noise contamination in all parts of the spectrum. In such cases, the derivatives and spectral moments of the system, mainly the variance and second derivative of $Z(\omega)$, become important as they describe its behaviour. The information conveyed in these functions is valuable when frequency variations are very rapid. In our presentation of sites 1 and 2 no low-frequency decade 3 (1–0.1 Hz) and decade 4 (0.1–0.01 Hz) response functions have been shown. Decade 4 data were not collected for these sites, and decade 3 results simply *do not exist*; the noise sources have been formidable for both FFT- and MAXENT-based analyses. The MAXENT procedure however has a further advantage in that it can handle short data lengths without significant loss of stability in the spectral estimates (e.g. Beamish & Tzanis 1986; Tzanis & Beamish 1987). For the data in question, the duration of the noise sources (0.1–1 Hz) was less than the time interval of individual data windows. An attractive way to circumvent such noise problems, therefore, would appear to be the processing of short time windows. Our data were divided so that each $N = 150$ window provided three $N = 50$

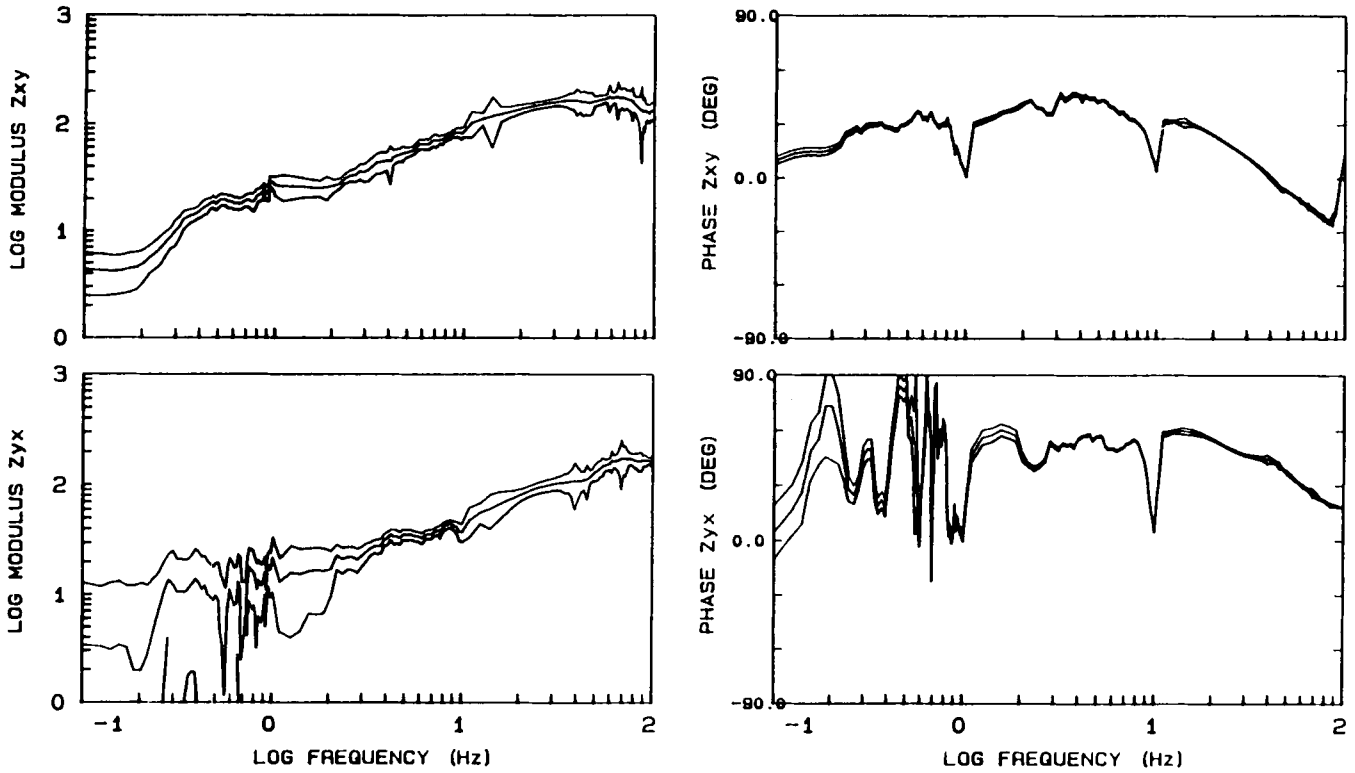

Figure 7. The high-resolution impedance function for three decades of data at example site 1. Impedance in units of mV km^{-1} nT^{-1}. Decade 1 (100–10 Hz) response is the same as in Fig. 2(b). Decade 2 (10–1 Hz) and decade 3 (1–0.1 Hz) responses are recalculated from reduced length ($N = 50$) data windows, with an AR operator of order $M = 6$.

reduced length windows. The sample space, increased by threefold, was then subjected to MAXENT spectral analysis with an AR filter of order 6. The procedure was repeated for decade 2 as well, and the results for site 1 are shown in Fig. 7. One can immediately see a significant improvement in the estimation of decade 2, particularly the 1–3 Hz band when compared with Fig. 2(a). The decade 3 response is at last estimated but displays extremely unstable characteristics, with the noise obviously more intense in the Z_{yx} component.

5 SMOOTHING A HIGH-RESOLUTION RESPONSE FUNCTION

The three-decade response of Fig. 7 provides a good example of an impedance function displaying rapid frequency variation and therefore its alternative description as a high-order polynomial can be acknowledged.

All the piecewise-discontinous portions imply an unphysical response. They do, however, contain some very important information; they tell us exactly how the contaminated response function behaves locally. Conventional analysis, by discretizing the observed impedance function, discards all such information. As a natural consequence, if smoothing of the response function is attempted, it will have to rely on curve fitting of the data with some numerical polynomial interpolation technique, as in Hobbs (1982) and others. This is, at least theoretically, unwarranted because these methods will fit to a polynomial approximation to the data, thus *imposing* on it structure with no *a priori* information. Parker (1983) objects to the use of conventional polynomial interpolations, arguing that they are inconsistent with the conditions for the existence of 1D conductivity distriutions (i.e. Weidelt's (1972) inequality constraints). This is quite a strong point, because the interpolating polynomial may not possess the necessary analytical properties, thereby violating causality. This point is also raised by Claerbout (1976, p. 62) who, however, admits that in many practical situations such approximations can be inconsequential. The only theoretically valid interpolations, are those that involve the formal expressions for the polynomial Earth response (e.g. Khachay 1978; Parker & Whaler 1981). The methods of the above authors are guaranteed to succeed, but require some computational effort, especially in the case of a highly resolved response function. We agree that a smoothing procedure should not violate causality. Therefore, we feel that it is important to use the information contained in the observed response in order to improve our estimation without imposing some kind of structure. This information can, in general, be extracted from a complete sounding curve and its derivatives.

Consider the function

$$F(\omega) = u(\omega)a^{\omega}, \qquad u(\omega) = \begin{cases} 1, & \omega > 0 \\ 0, & \omega < 0 \end{cases}$$

for real ω. The observed function $Z(\omega)$ can be convolved with $F(\omega)$ to obtain

$$S(\omega) = (2\pi)^{-1} \sum_{n=1}^{N} Z(\omega + \omega_n)F(\omega_n). \tag{6}$$

This frequency domain convolution is permissible because $F(\omega)$ is analytic over the entire real ω-axis; $Z(\omega)$ is analytic over the real ω-axis, and by the Cauchy–Goursat theorem its derivatives are likewise analytic and defined over the entire real ω-axis. Equation (6) defines a weighted moving summation over the real axis of the ω-plane; in contrast to conventional averaging techniques, it defines a quasi-continuous operation, adaptive to the constantly varying frequency characteristics of $Z(\omega)$. The convolution (6) exhibits several useful properties. Take for instance the integral form

$$S = (2\pi)^{-1} \int_{\omega_0}^{\omega_N} Z(\omega)a^{\omega}\, d\omega. \tag{7}$$

With the condition that $Z^{(n+1)}(\omega) = 0$, it can be shown that (7) reduces to the finite series expansion

$$2\pi S = a^{\omega_0} \sum_{n=1}^{N} \frac{Z^{(n)}(\omega_0)}{|\ln(a)|^{(n+1)}} \tag{8}$$

in terms of the derivatives $Z_{ij}^{(n)}(\omega)$ of the tensor elements $Z_{ij}(\omega)$. The value of S is evaluated on ω_0, i.e. (7) is simply an integral form of a single step of the complete convolution operation (6), and comprises the output at a single frequency ω_0. Therefore, the value of S, $S(\omega_0)$ can be thought of as the prediction of $Z(\omega_0)$, given a value of a. It follows that we are interested in the particular value that minimizes the error variable $X(\omega_0) = Z(\omega_0) - S(\omega_0)$. This is a 'filtering' problem, with an easy solution, since there exists only one variable (a) in the 'filter' sequence a^{ω}.

Another useful property of (6) becomes apparent when we consider the properties of $F(\omega)$ in the time domain. For the case $0 < a < 1$, (6) corresponds to a multiplication of the impulse response with a time function of the form

$$2\pi f(t) = [|\ln a| - (-it)] \cdot [|\ln a|^2 + t^2]^{-1} \tag{9}$$

the inverse Fourier transform of $F(\omega)$. The factor $(-it)$ is the Fourier frequency differentiation operator. The numerator of (9) will damp $Z(\omega)$ by a factor $|\ln a|$ while the negative sign ensures that the phase remains unchanged during differentation. Note that the derivative of a polynomial is a polynomial of a lesser degree, i.e. a smoother function. More importantly however, the factor $(|\ln s|^2 + t^2)$ in the denominator of (9) damps the trailing coefficients of the impulse response, thus forcing on it a minimum-delay property. Large trailing coefficients are responsible for non-minimum phase variations since their magnitude is related to the effects of maximally dispersed (non-causal) processes. Thus (9) produces a combination of differentiation and weighting that both lead to a smoother function. From the above it can be seen that we are essentially dealing with a time domain process; the crucial weighting function in (9) is left to the time variable t.

The frequency domain convolution (6), as it stands, is a very ineffective operation; ω may vary within ranges of several decades, so that a needs to be different for various frequency bands (i.e. $a > 1$ if $\omega < 1$, and $a < 1$ if $\omega > 1$). Therefore it cannot be applied easily, and certainly not for values of ω near unity. The problem is overcome if we transform (6) to the discrete form

$$S_i = (2\pi)^{-1} \sum_{j=1}^{N} Z_{i-j}F_j \tag{10}$$

with $F_j = a^j$, $j = 1, 2, 3 \ldots$ Then, the condition $a < 1$ ensures that the weight series will decay fairly rapidly, so that only local frequency estimates will be included in the summation. The smoothing operation as applied through (10) becomes universal and can be used to process wide-band as well as narrow-band response functions. The optimum value of a will lie in a quite narrow range and will be data (noise) dependent; in our experience it is approximately bounded as $0.82 < a < 0.94$.

An example of the technique applied to noisy field data is now given. Fig. 8(a) shows 3 decades of the unrotated off-diagonal tensor elements recorded in an intense noise environment (example site 6). Here, the effects of closely spaced noise sources are clearly observed in the extreme variance of the resulting response function, particularly in decades 2 and 3. The net effect can easily be perceived as a random process superimposed on the true impedance and additional systematic perturbations, e.g. Feature 1. The gaps in the components of the sounding curves near 50 Hz correspond to frequency estimates that did not pass the acceptance criteria. Fig. 8(b) shows the impedance function recovered after only 1 iteration with $a = 0.87$. Apart from the overall improvement, other detailed effects include the recovery of the response mismatch near the decade 3 and 2 Nyquists (0.1 and 1 Hz, respectively) and a partial, although not completely satisfactory, reduction of the magnitude of Feature 1 in the phase response. It appears that the technique is also an effective interpolator. Note however

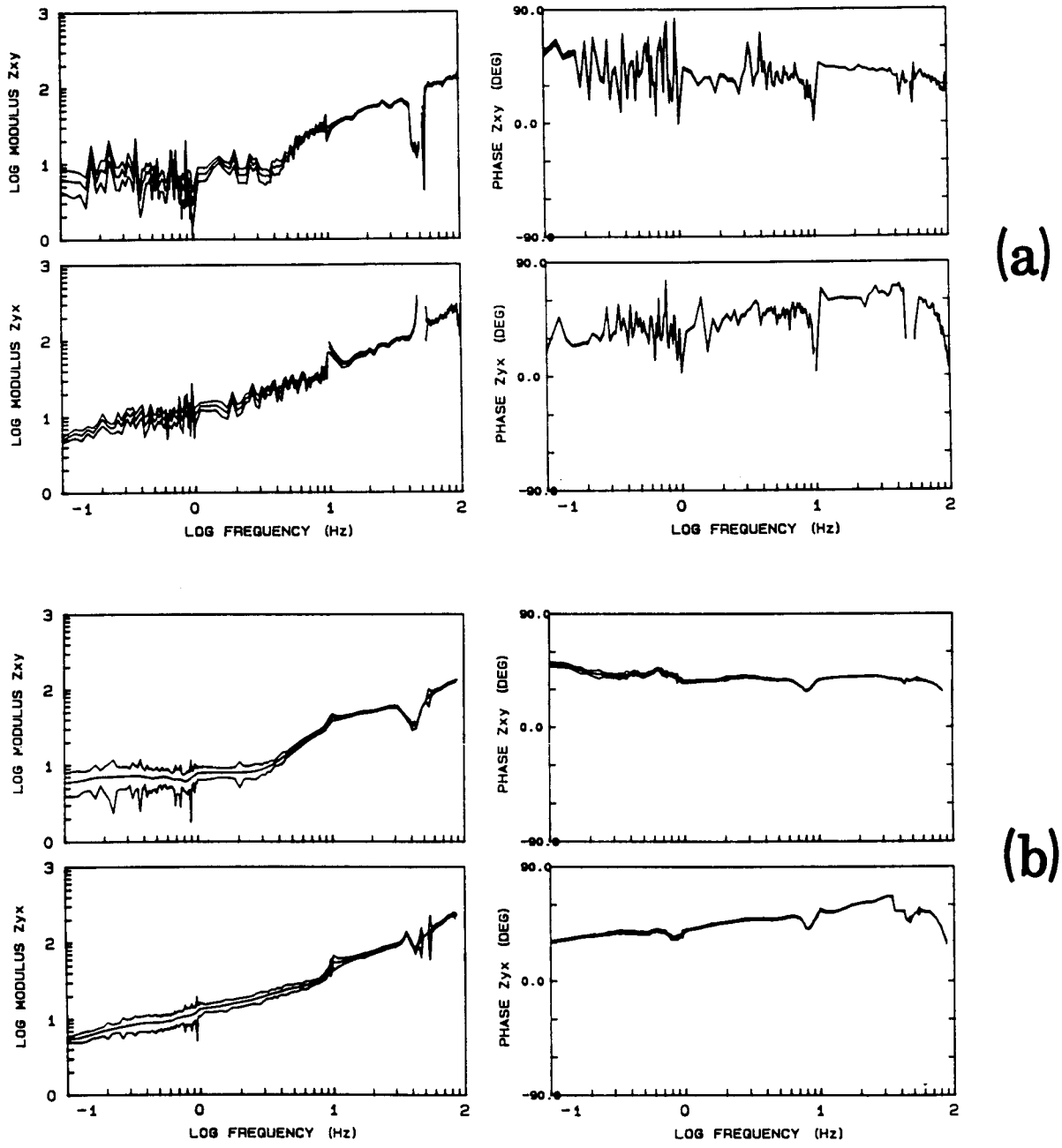

Figure 8. The high-resolution impedance function for three decades of data at example site 6. Impedance in units of $\mathrm{mV\,km^{-1}\,nT^{-1}}$. (a) The unstable impedance function due to intense noise. (b) The same impedance function after frequency domain smoothing (one iteration).

that if long gaps exist within the data, the technique cannot readily cope (e.g. the 50 Hz feature in the Z_{yx} element). Likewise, if large-scale inconsistencies exist in the data, the technique should be applied with caution.

The results for site 1 are presented in Fig. 9(a). In this case, the extremely unstable nature of the observed decade 3 function demands a separate initial treatment. This was done with an optimum weight of $a = 0.93$. Subsequently, the 3 decades were treated as a whole, and the result shown is after 1 iteration, with $a = 0.86$. In this case as well, the smoothing process is unable to totally remove Feature 1, although the reduction of its magnitude is quite dramatic. The 1–3 Hz determination of the decade 2 response appears to have improved. Note however that the reliable recovery of the decade 3 amplitude response over the 0.1–0.4 Hz bandwidth is questionable. With no *a priori* information about the Earth structure and in the absence of lower frequency impedance determinations, it is impossible to say whether the 'smoothed' function is physical or not, the local steep gradients contradict the intuitively smooth nature of a low degree polynomial response. The same is probably true for the 1–3 Hz decade 2 estimates as well. What is important here, however, is that the recovered phase appears to be more reliable for parts of the bandwidth at least. In Fig. 9(b) we present the phase 'cleaned' from the residual perturbations and 'conspicuous' bands. If one decides to make use of decade 3 information, the remaining phase estimates will provide enough constraints for inversion and modelling.

In view of the foregoing discussion, we note that in cases

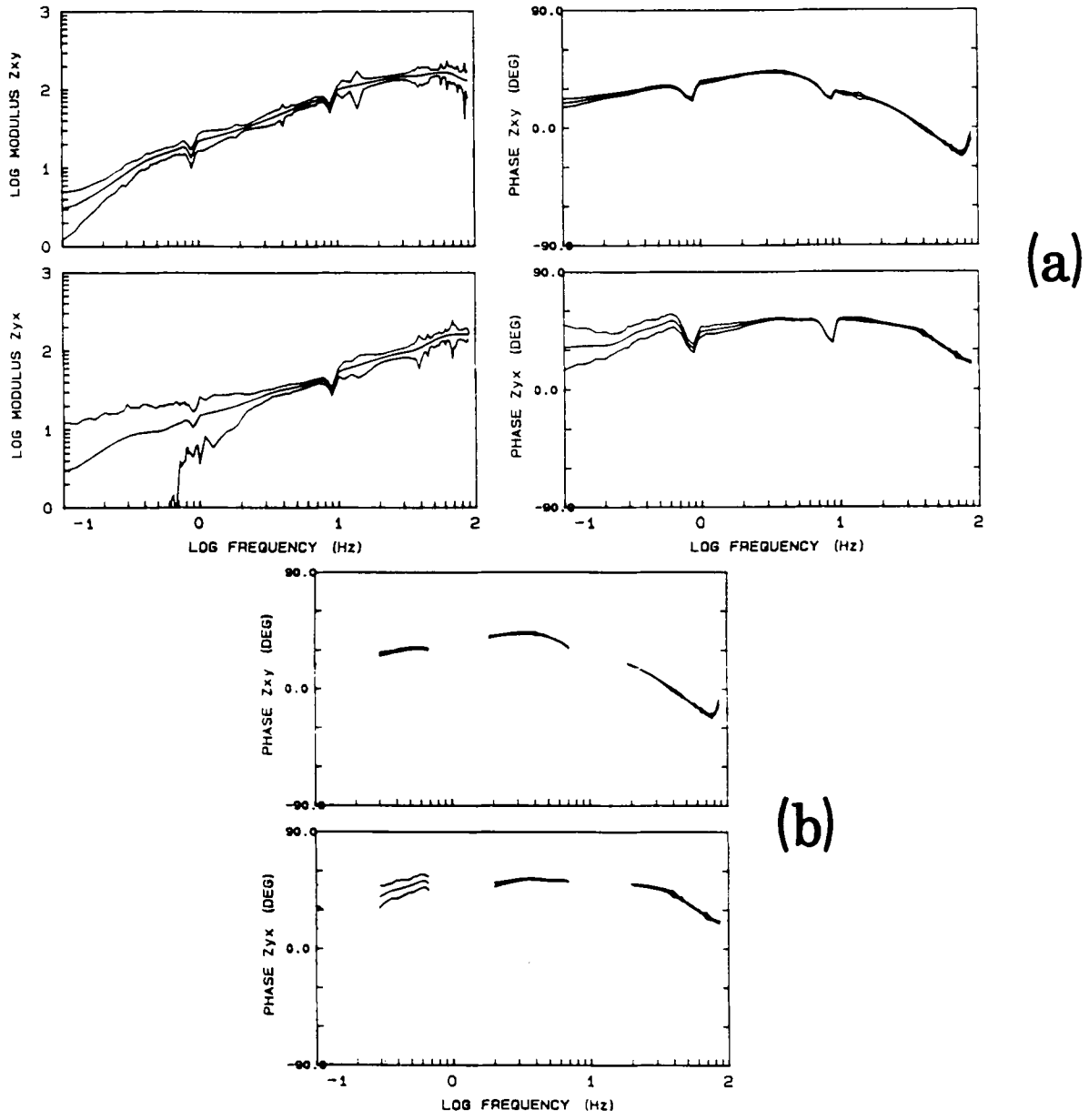

Figure 9. The high-resolution impedance function for 3 decades of data at example site 1, with frequency domain smoothing. Impedance in units of mV km^{-1} nT. (a) The smoothed impedance function of Fig. 7. (b) The phase of the smoothed impedance function of Fig. 9(a), with the remaining unstable and/or conspicuous spectral segments removed.

of severe noise contamination, we may be content with the recovery of either a smooth amplitude or phase response function, that the combination of the high-resolution estimation and the adaptive smoothing technique facilitates. Either quantity will invert satisfactorily if it is reliable, and also it is always possible to reconstruct the amplitude of $Z(\omega)$ (or the apparent resistivity) from its phase and vice versa, for they constitute Hilbert transforms of each other. This is a consequence of the causality requirement, mathematically expressed with the Krammers–Kronig dispersion relations (e.g. Weidelt 1972; Fischer & Schnegg 1980). Weidelt (1972) gives a method for the recovery of the phase from the resistivity. A very interesting algorithm for the calculation of an unbiased (and also non-statically shifted) amplitude response from a smooth phase response is given in Clay & Hinich (1981), following the analysis of Boehl & Bostick (1977). In their treatment, resolution plays an important role since the numerical stability of the procedure depends on it.

6 CONCLUSION

In our introduction of the concept of frequency resolution in relation to MT data analysis, we have been primarily concerned with the study and understanding of contaminated AMT observations. Highly resolved impedance functions display detailed properties as a function of frequency. Thus, comparisons of spectral features facilitate the correlation of noise effects, not only for single site impedance determinations but for regionally collected data as well. These comparisons are at least as difficult with the conventional FFT-based spectral approach. As we have shown, there may exist situations for which the subtle low-intensity noise sources may prove to be more insidious than intense, directly identifiable (and removable in most cases) interference. We believe that such comparisons provide a valuable interpretational aid because, despite being subjective and difficult to quantify, they enable a detailed view of the data quality and what is to be expected of it.

We have also made use of the mathematical properties of a contaminated polynomial Earth response function in order to study a technique that will smooth its perturbations. The reasoning we follow stems from the fact that passive EM induction is a continuous process, and arbitrary frequency discretization may sometimes impose conflicting influences on a response function and therefore much of the information it contains may be lost. We have tried to manipulate this information to our advantage with, we believe, some success. Moreover, in our example for decade 3 of site 1, we have used the short data handling capacity of MAXENT in association with its resolution capacity to extract stable determinations of portions of the impedance function. We believe that such a facility is very important and must be taken into consideration when processing heavily distorted data.

Note, however, in view of the above discussion, that we *do not* advocate that high-resolution estimation should become standard in EM data analysis. The spectral techniques associated with high-resolution require considerable computatonal effort that limits their in-field processing capacity for most existing (high frequency) data acquisition systems. When time is not a critical factor, however, and the data appear conspicuous, the implementation of such techniques may assist in the solution of several problems associated with response function estimation.

A final comment concerns the effects of the variation of the order (M) of the autoregressive (AR) process fitted to the data. We have consistently used standard lengths of $M = 10$ and $M = 6$ for data lengths of $N = 150$ and $N = 50$, respectively, and one may argue that these may not be optimum for all the data subsets. Although the problem of the optimum predictor length is an important and long-standing one in the statistical literature, varying M has no large-scale effects on response function estimation which is concerned with spectral ratios. We have found that any length of the order of 10 per cent of the data but not less than 5 per cent will produce comparable results. Empirically a lower limit of M follows from our discussion of the polynomial representation of $Z(\omega)$. We therefore suggest that for a given data bandwidth the lowest AR order sufficient to resolve $Z(\omega)$ is at least equal to the degree of $Z(\omega)$.

ACKNOWLEDGMENTS

The data collection was supported by the Natural Environment Research Council, the Overseas Development Administration and Kandilli Observatory, Bogazici University. The authors thank the referees and the associate editor whose comments have contributed to a much improved manuscript. This paper is published with the permission of the Director, British Geological Survey (NERC).

REFERENCES

Beamish, D. & Tzanis, A., 1986. High resolution spectral characteristics of the Earth-ionosphere cavity resonances, *J. atmos. terr. Phys.*, **48**, 187–203.

Bliokh, H., Nikolaenko, A. P. & Filippov, Yu. F., 1980. *Schumann resonances in the Earth-Ionosphere Cavity*, IEE Electromagnetic Wave Series 9, P. Peregrinus Ltd, Stevenage.

Boehl, J. E. & Bostick, F. X., 1977. An application of the Hilbert transform to the magnetotelluric method, *PhD thesis*, University of Texas at Austin.

Burg, J. P., 1975. Maximum entropy spectral analysis, *PhD thesis*, Stanford University, Stanford, California.

Chave, A. D., Thomson, D. J. & Ander, M. E., 1987. On the robust estimation of power spectra, coherences and transfer functions, *J. geophys. Res.*, **92**, 633–648.

Claerbout, F. J., 1976. *Fundamentals of Geophysical Data Processing with Applications to Petroleum Prospecting*, McGraw-Hill, New York.

Clay, C. S. & Hinich, M. J., 1981. Estimating the Earth's impedance function when there is noise in the electric and magnetic signals, in *Applied Time Series Analysis II*, ed. Findley, D. F., Academic Press, New York.

Fischer, G. & Schnegg, P. A., 1980. The dispersion relations of the magnetotelluric response and their incidence on the inversion problem, *Geophys. J. R. astr. Soc.*, **62**, 661–673.

Hobbs, B. A., 1982. Automatic model finding for the one-dimensional magnetotelluric problem, *Geophys. J. R. astr. Soc.*, **68**, 253–264.

Jaynes, E. T., 1982. On the rationale of maximum entropy methods, *Proc. IEEE*, **70**, 939–952.

Khachay, O. A., 1978. On solving the inverse problem of magnetotelluric sounding for a complex impedance, *Phys. Solid Earth, Izvestiya*, **14**, 896–900.

Menvielle, M. & Szarka, L., 1986. Distortions of electromagnetic fields: topographic and man-made, Review paper presented at

the *VIII IAGA Workshop on Electromagnetic Induction*, Neuchatel, Switzerland.

Parker, R. L., 1983. The magnetotelluric inverse problem, *Geophys. Surv.*, **6**, 5–25.

Parker, R. L. & Whaler, K. A., 1981. Numerical methods for establishing solutions to the inverse problem of electromagnetic induction, *J. geophys. Res.*, **86**, 9574–9584.

Robinson, E. A., 1967. *Multichannel Time Series Analysis with Digital Computer Programs*, Holden-Day, San Francisco.

Robinson, E. A., 1980. *Physical Applications of Stationary Time Series*, Griffin, London.

Sims, W. S., Bostick, Jr, F. X. & Smith, H. W., 1971. The estimation of magnetotelluric impedance tensor elements from measured data, *Geophysics*, **36**, 938–942.

Strand, O. N., 1977. Multichannel complex maximum entropy (autoregressive) spectral analysis, *IEEE Trans. Automatic Control*, **AC-22**, 634–640.

Tzanis, A. & Beamish, D., 1987. Audiomagnetotelluric crustal sounding using the Schumann resonances, *J. Geophys.*, **61**, 97–100.

Tzanis, A., 1987. Investigations on the properties and estimation of earth response operators from EM sounding data, *PhD thesis*, University of Edinburgh.

Weidelt, P., 1972. The inverse problem of geomagnetic induction, *Z. Geophys.*, **38**, 257–289.